

## Contrasting Ocean–Atmosphere Dynamics Mediate Flood Hazard across the Mississippi River Basin<sup>©</sup>

SAMUEL E. MUÑOZ<sup>ID</sup>,<sup>a,b</sup> BRYNNYDD HAMILTON,<sup>a</sup> AND B. PARAZIN<sup>a</sup>

<sup>a</sup> Department of Marine and Environmental Sciences, Marine Science Center, Northeastern University, Nahant, Massachusetts

<sup>b</sup> Department of Civil and Environmental Engineering, Northeastern University, Boston, Massachusetts

(Manuscript received 6 June 2022, in final form 20 September 2022)

**ABSTRACT:** The Mississippi River basin drains nearly one-half of the contiguous United States, and its rivers serve as economic corridors that facilitate trade and transportation. Flooding remains a perennial hazard on the major tributaries of the Mississippi River basin, and reducing the economic and humanitarian consequences of these events depends on improving their seasonal predictability. Here, we use climate reanalysis and river gauge data to document the evolution of floods on the Missouri and Ohio Rivers—the two largest tributaries of the Mississippi River—and how they are influenced by major modes of climate variability centered in the Pacific and Atlantic Oceans. We show that the largest floods on these tributaries are preceded by the advection and convergence of moisture from the Gulf of Mexico following distinct atmospheric mechanisms, where Missouri River floods are associated with heavy spring and summer precipitation events delivered by the Great Plains low-level jet, whereas Ohio River floods are associated with frontal precipitation events in winter when the North Atlantic subtropical high is anomalously strong. Further, we demonstrate that the El Niño–Southern Oscillation can serve as a precursor for floods on these rivers by mediating antecedent soil moisture, with Missouri River floods often preceded by a warm eastern tropical Pacific (El Niño) and Ohio River floods often preceded by a cool eastern tropical Pacific (La Niña) in the months leading up peak discharge. We also use recent floods in 2019 and 2021 to demonstrate how linking flood hazard to sea surface temperature anomalies holds potential to improve seasonal predictability of hydrologic extremes on these rivers.

**KEYWORDS:** North America; Flood events; Atmosphere–ocean interaction; ENSO; Climate variability

### 1. Introduction

The Mississippi River basin is the largest drainage network in North America; predicting high flows along its rivers is critical for navigation, infrastructure planning, flood mitigation, and emergency response. The Mississippi River and its major tributaries—the Ohio and Missouri Rivers—have long served as economic corridors for the transportation of goods, generation of hydroelectric power, and industrial and agricultural activity (Knox 2007). Flooding represents a perennial hazard that disrupts these activities (Camillo 2012), with the costs of recent flooding in 2019, for example, estimated to have exceeded \$20 billion in total economic losses (NCEI 2021). Despite their severe economic consequences, predicting flooding on these rivers remains challenging, with long-range probabilistic outlooks based on current and forecast hydrologic conditions providing a lead time of 1–3 months (Lincoln and Graschel 2016, 2018; NOAA 2016). One approach to extend and improve long-range forecasts involves using the connections between hydrologic

extremes and coupled modes of ocean–atmosphere variability (Hamlet and Lettenmaier 1999; Wang and Eltahir 1999; Schöngart and Junk 2007) that evolve gradually and control the influx and convergence of moisture to the North American continental interior (Ropelewski and Halpert 1986; Chen and Kumar 2002; Muñoz and Dee 2017).

Analyses of hydrologic extremes over midcontinental North America emphasize the roles of synoptic-scale features and sea surface temperature anomalies in generating both droughts and pluvials (Seager et al. 2005; Cook et al. 2007; Feng et al. 2011; Cook et al. 2011, 2014; Coats et al. 2016). Of particular interest for precipitation extremes in this region are the position and strength of the North Atlantic subtropical high (NASH; Li et al. 2011; Smith and Baeck 2015) and the strength of the Great Plains low-level jet (GPLLJ; Weaver and Nigam 2008; Dirmeyer and Kinter 2009, 2010; Zhang and Villarini 2019)—both of which regulate the advection of moisture from the Gulf of Mexico toward the Mississippi River basin. Relatedly, both the North Atlantic Oscillation (NAO) and Pacific–North American pattern (PNA), represent modes of atmospheric variability that mediate meridional moisture transport into the Mississippi River basin (Harding and Snyder 2015; Mallakpour and Villarini 2016; Malloy and Kirtman 2020). Through its influence on the position and strength of the polar and subtropical jets, El Niño–Southern Oscillation (ENSO) also influences precipitation patterns over the Mississippi River basin, with warm eastern equatorial Pacific sea surface temperatures (El Niño) enhancing winter and spring precipitation over the Great Plains and Gulf Coast and cool eastern equatorial Pacific sea surface temperatures (La Niña) enhancing

<sup>©</sup> Supplemental information related to this paper is available at the Journals Online website: <https://doi.org/10.1175/EI-D-22-0015.s1>.

*Corresponding author:* Samuel E. Muñoz, s.munoz@northeastern.edu

*Earth Interactions* is published jointly by the American Meteorological Society, the American Geophysical Union, and the Association of American Geographers.

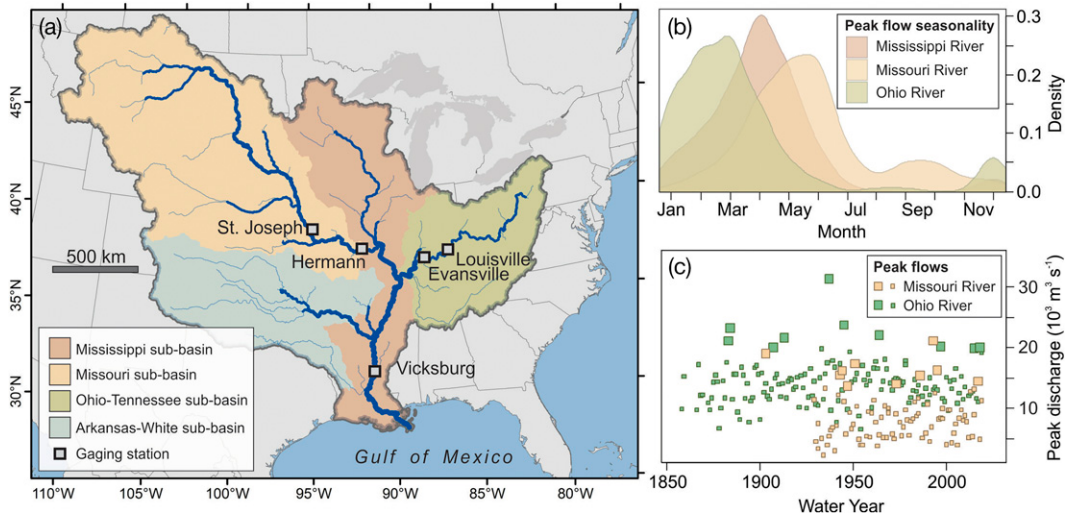


FIG. 1. The Mississippi River basin and its principal tributaries: (a) major subbasins of the Mississippi River basin and gauging stations referred to in the main text; (b) seasonal timing of peak annual discharges of the lower Mississippi River (Vicksburg gauge 07289000), Missouri River (Hermann gauge), and Ohio River (Louisville gauge) expressed as a density function of all water years in the instrumental record; (c) peak annual discharges from the Missouri River at Hermann and Ohio River at Louisville for water years 1850–2017, with larger symbols denoting the largest 10 events at each gauge.

precipitation over the Ohio River valley (Ropelewski and Halpert 1986; Thomson et al. 2003). At the same time, sea surface temperature anomalies over the North Atlantic have also been associated with mediating streamflow near the outlet of the Mississippi River basin through its influence on the position and strength of the North Atlantic subtropical high (Enfield et al. 2001; Muñoz et al. 2018). These features and related atmospheric and oceanic mechanisms have been variously ascribed to historic flood events on the Missouri (Parrett et al. 1993; Kunkel et al. 1994; Arritt et al. 1997; Dirmeyer and Kinter 2009; Hoerling et al. 2013), Ohio, and lower Mississippi Rivers (Lott and Myers 1956; Nakamura et al. 2013; Therrell and Bialecki 2015; Smith and Baeck 2015), although the importance and timing of different mechanisms on these tributaries remains unclear. As a result, a unified model describing how hydrologic extremes on the major tributaries of the Mississippi River basin are mediated by ocean–atmosphere variability has yet to emerge.

Here, we examine the atmospheric and oceanic circulation patterns that generate large floods on the principal tributaries of the Mississippi River basin using a climate reanalysis and river gauge data. We focus on all of the largest observed floods (recurrence period  $\geq 10$  years) for the period 1870–2018 on the lower reaches of the Missouri and Ohio Rivers to evaluate the large-scale atmosphere–ocean conditions that contribute to major floods on these rivers. We show that the seasonality and atmospheric mechanisms that trigger floods on these two tributaries differ. Further, we propose that the state of ENSO mediates antecedent moisture over these subbasins and often serves as a precursor for enhanced flood hazard on the major tributaries of the Mississippi River Basin. We also evaluate recent floods that primarily affected the Missouri–Mississippi Rivers (2019) and Ohio River (2021) to illustrate the contrasting conditions that preceded these floods.

## 2. Data and method

### a. Hydrologic datasets

River discharge and stage data are obtained from the U.S. Geological Survey (USGS) water data for the nation (USGS 2021). We extracted peak annual discharges from gauges with relatively long and continuous records on the lower reaches of the targeted rivers—namely, the Missouri River at Hermann, Missouri (USGS gauge 06934500), and Ohio River at Louisville, Kentucky (gauge 03294500) (Fig. 1). These gauges include historic peaks back to 1844 on the Missouri River and 1832 on the Ohio River, although here we limit our analyses to events after 1870 because of the limited availability and reliability of reanalysis data and gridded observations before this time (Slivinski et al. 2019). We computed the empirical recurrence interval for all annual discharge maxima between 1870 and 2017 using

$$\text{recurrence interval} = (n + 1)/m,$$

where  $n$  is the total number of annual maxima in the gauge and  $m$  is the rank (in descending order) of the event. We then selected all events with recurrence intervals of  $>10$  years at each gauge, and focused subsequent analyses on these flood events (Table 1). We focus on floods with recurrence intervals of  $\geq 10$  years to isolate the atmospheric and oceanic processes that mediate the largest events on these rivers. These flood events rank among the largest floods by discharge since 1870 at other long gauge records on the lower reaches of the targeted tributaries, including the Missouri River at Saint Joseph (06818000) and Ohio River at Evansville (0332200), and thus are considered to be representative of large floods on the lower Missouri and Ohio Rivers. To more closely examine

TABLE 1. Largest floods (recurrence interval  $\geq 10$  years) by peak daily discharge on the Missouri River at Hermann and Ohio River at Louisville from 1870 to 2017.

Event No.	Missouri River at Hermann			Ohio River at Louisville		
	Peak date	Peak discharge ( $m^3 s^{-1}$ )	Recurrence interval (yr)	Peak date	Peak discharge ( $m^3 s^{-1}$ )	Recurrence interval (yr)
1	31 Jul 1993	21 240	91	26 Jan 1937	31 430	148
2	7 Jun 1903	19 820	46	7 Mar 1945	23 870	74
3	19 Jul 1951	19 140	30	16 Feb 1884	23 360	50
4	19 May 1995	17 500	23	12 Mar 1964	22 230	37
5	28 Apr 1944	16 400	18	2 Apr 1913	21 780	30
6	21 May 1943	16 340	15	16 Feb 1883	21 240	25
7	5 Oct 1986	15 570	13	6 Mar 1997	20 270	21
8	4 May 2017	15 550	12	22 Jan 1907	20 190	19
9	25 Apr 1973	14 580	11	16 Mar 2015	19 990	16
10	29 Jun 1947	14 160	10	23 Mar 1933	19 990	15

the recent 2019 and 2021 floods, we extracted peak stage and discharge data from all gauges within the Mississippi River basin for the water year (e.g., 1 October 2018–30 September 2019 for the 2019 water year) and classified each gauge's peak annual stage based on its stage category (e.g., major flood stage or moderate flood stage).

#### b. Atmospheric and oceanic datasets

To examine the atmospheric patterns associated with the largest observed floods, we examined geopotential height and winds from the National Centers for Environmental Prediction (NCEP) Twentieth Century Reanalysis, version 3 (V3; [Slivinski et al. 2019](#)). For each flood event, we extracted daily 850 hPa geopotential heights,  $u$  wind,  $v$  wind, soil moisture, precipitation, and runoff for the 30 days preceding the flood and computed a standard score anomaly based on a long-term mean and standard deviation for the period 1981–2010. We examined aggregate behavior for each tributary by computing the mean of geopotential height, wind, soil moisture, precipitation, and runoff anomalies prior to all events for a given tributary and expressing these anomalies in terms of standard deviations  $\sigma$  from the mean. We computed the significance of these anomalies by bootstrapping with 10 000 random samples of the same length drawn from each variable and used the resulting distribution to estimate the 10th and 90th percentiles. We also used the meridional wind field from the V3 reanalysis to compute a daily GPLLJ index that is based on the method described in [Weaver and Nigam \(2008\)](#) (i.e., 850-hPa meridional wind anomaly in the core GPLLJ region of  $25^{\circ}$ – $35^{\circ}$ N,  $102^{\circ}$ – $97^{\circ}$ W) and examined the aggregate (mean) behavior of the GPLLJ in the 60 days before and after flood events. We also obtained a daily NAO index from [Cropper et al. \(2015\)](#) and [Hurrell et al. \(2003\)](#) and examined aggregate behavior of the NAO in the 60 days before and after flood events on each tributary. We also used the Extended Reconstructed Sea Surface Temperature (ERSST v5; [Huang et al. 2017](#)) to examine sea surface temperature anomalies associated with flood events, specifically on the Niño-3.4 index, which we calculated using the method described by [Trenberth \(1997\)](#). To compute the significance of these aggregate anomalies,

we used bootstrapping in which 10 000 random samples were drawn from the indices and estimated the 10th and 90th percentiles of the resulting distributions.

### 3. A tale of two tributaries

The Missouri and Ohio Rivers—the two major tributaries of the Mississippi River basin—respectively drain the western and eastern portions of the basin and differ in their physiography and hydroclimatology ([Fig. 1a](#)). To the west, the Missouri River basin is bounded by the Rocky Mountains and is characterized by the continental and semiarid climate of the Great Plains ([Wise et al. 2018](#)). Within the Missouri River basin, total annual precipitation decreases with distance from the Gulf of Mexico, ranging from  $\sim 80$  cm near the Missouri River's confluence with the Mississippi River at Saint Louis, Missouri, to  $\sim 40$  cm near the Missouri River headwaters near Helena, Montana ([Knox 2007](#)). Temperature and precipitation patterns of the Missouri River basin are characterized by strong seasonal contrasts in temperature and precipitation, with 60%–80% of total annual precipitation delivered during the warm spring and summer months (March–August) ([Muñoz et al. 2020](#)). In contrast, much of the Ohio River basin is characterized by a humid subtropical climate with mild winter temperatures and higher total annual precipitation (100–120 cm) that is distributed more evenly throughout the year ([Knox 2007](#)). The Ohio River basin is bounded to the east by the Appalachian Mountains, with the Ohio River itself draining into the lower Mississippi River at Cairo, Illinois—roughly 240 km downstream from the confluence of the Missouri and upper Mississippi Rivers.

As a result of their hydroclimatic contrasts, the Ohio and Missouri Rivers differ in the seasonality ([Fig. 1b](#)) and magnitude ([Fig. 1c](#)) of their peak flows. Peak annual flows on the lower Ohio River tend to occur in the winter or early spring, with the 10 largest historic floods at Louisville cresting between January and April ([Table 1](#)). Floods on the Missouri River, in contrast, tend to occur in the spring or summer, with the largest events at Hermann cresting between May and October. Streamflow on the Missouri and Ohio Rivers is influenced by infrastructure ([Smith and Winkley 1996](#); [Pinter et al.](#)

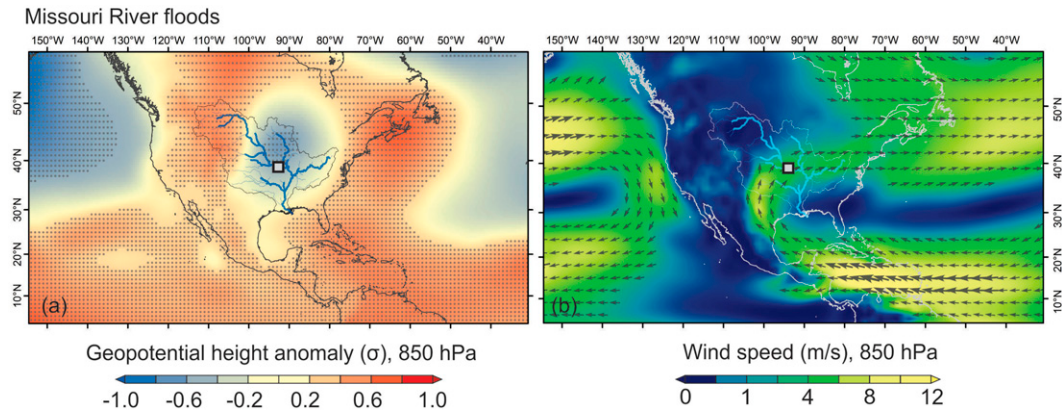


FIG. 2. Lower-atmospheric dynamics in the month prior to peak discharge for the 10 largest floods on the lower Missouri River: (a) geopotential height anomaly (850 hPa) and (b) winds (850 hPa). Gray boxes denote locations of the gauge used to define floods. Geopotential height and wind speeds are expressed as standardized anomalies in terms of standard deviations  $\sigma$  from the long-term monthly mean (1981–2010). Stippling in (a) denotes composite anomalies that exceed the 90% confidence interval.

2008), particularly by the presence of dams and reservoirs on the upper Missouri River (Wise et al. 2018). An east-to-west precipitation gradient across the Mississippi River basin ensures that the Ohio River—despite its basin encompassing only ~15% of the total Mississippi River basin—is associated with higher magnitude peak flows than the Missouri River and is the dominant contributor of discharge to the Mississippi River (Keown et al. 1986). The seasonality of peak annual flows on the lower Mississippi River tends to follow those of the Ohio River, occurring predominantly in spring (March–May). These hydroclimatic contrasts among the major tributaries of the Mississippi River basin are reflected in the different atmospheric and oceanic circulation patterns that precede major flood events on these rivers, which we examine next.

#### 4. Hydrometeorological mechanisms that generate floods

The atmospheric circulation patterns associated with the largest historical floods on the lower Missouri and Ohio Rivers promote advection and convergence of moisture from the

Gulf of Mexico toward the continental interior, but the mechanisms that generate this process differ among the lower Missouri River (Fig. 2) and Ohio River (Fig. 3). For lower Missouri River floods (Fig. 2), aggregate atmospheric behavior in the month of the 10 largest historical floods exhibits a region of anomalously low geopotential height in the lower troposphere (850-hPa level) centered over the Mississippi River basin (Fig. 2a). These geopotential height patterns are accompanied by a directed stream of lower-level winds flowing from the Caribbean Sea and Gulf of Mexico (Fig. 2b) that closely resembles the Great Plains low-level jet (Higgins et al. 1997; Weaver and Nigam 2008) and converges over the Missouri River basin to produce precipitation over the Missouri River and upper Mississippi River basins (Harding and Snyder 2015; Malloy and Kirtman 2020). This atmospheric pattern, characterized by a zonally aligned wave train with significant low geopotential height anomalies over the North Pacific, Mississippi River basin, and North Atlantic, is similar to the “Maya Express” (Dirmeyer and Kinter 2009) and “Midwest Water Hose” (Zhang and Villarini 2019) that

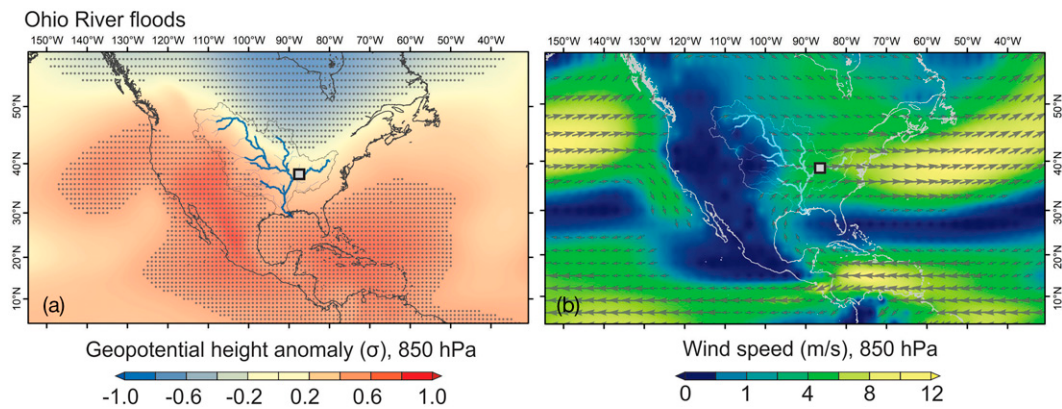


FIG. 3. As in Fig. 2, but for the lower Ohio River. (a) geopotential height anomaly (850 hPa) and (b) winds (850 hPa).

generate heavy precipitation events and flooding in the mid-western United States (Weaver and Nigam 2008; Dirmeyer and Kinter 2010; Malloy and Kirtman 2020). These enhanced low-level jet events occur in the spring and summer months, represent a major source of warm-season moisture to the mid-continent (Helfand and Schubert 1995; Mo et al. 1997; Wang and Chen 2009; Algarra et al. 2019), and have been directly linked to lower Missouri River flood events in 1993 and 2008 (Dirmeyer and Kinter 2009). Our analyses link this same mechanism to other large floods of the lower Missouri River, demonstrating that it precedes the majority of the largest of these floods (Fig. S1 in the online supplemental material) and is expressed in the aggregate of all large historical floods.

In contrast to the large-scale atmospheric patterns associated with floods on the lower Missouri River, aggregate behavior for the 10 largest lower Ohio River floods exhibit a low geopotential height anomaly (850-hPa level) over northern North America and high geopotential height anomalies over the North Pacific and North Atlantic that extend into the western United States and Mississippi River basin (Fig. 3). These patterns are consistent with strengthened subtropical highs and a positive NAO (Hurrell et al. 2001) that generate lower-level winds that flow from the Caribbean Sea and Gulf of Mexico toward the continental interior and converge over the southeastern United States (Fig. 3b) to generate precipitation over the Ohio River and lower Mississippi River basins. An anomalously strong and westerly position of the NASH is present in the month preceding the majority of the largest lower Ohio River floods examined here (Fig. S2 in the online supplemental material) and has previously been attributed to major floods on the lower Mississippi and Ohio Rivers, including the 2011, 1927, and 1937 floods (Lott and Myers 1956; Therrell and Bialecki 2015; Smith and Baeck 2015). The 1937 event is the flood of record for the lower Ohio River and is integrated into our analyses (Table 1), whereas the 2011 and 1927 events were largely confined to the lower Mississippi River (Camillo 2012) and were not among the largest events on the lower Ohio River. Our analyses show that this same mechanism—anomalously strong subtropical highs that promote meridional flow off the Gulf of Mexico and convergence over the midcontinent—serves as a trigger for floods on both the lower Ohio and Mississippi Rivers.

The contrast in the seasonality and atmospheric mechanisms that generate floods between the major western (Missouri River) and eastern (Ohio River) tributaries is also expressed in anomaly fields of key hydrologic variables including precipitation, soil moisture, and runoff (Fig. 4). In the month preceding major floods on the lower Missouri River, significant positive anomalies in precipitation, soil moisture, and runoff are situated over the upper Mississippi and Missouri River subbasins, while the Ohio River basin does not experience anomalously wet conditions during these events (Figs. 4a–c). In contrast, significant and positive precipitation, soil moisture, and runoff anomalies shift east to encompass the Ohio River and lower Mississippi River subbasins in the month preceding major floods on the lower Ohio River (Figs. 4d–f). These findings connect the contrasting atmospheric processes associated with floods on the major tributaries of the Mississippi River

system to the convergence of atmospheric moisture (precipitation), soil water storage, and runoff.

Our analyses of geopotential height, wind, precipitation, soil moisture, and runoff fields illustrate the hydrometeorological patterns that directly precede large floods on the major tributaries of the Mississippi River basin: On the lower Missouri River, the month leading up to a flood is characterized by a strengthened GPLJJ and positive moisture anomalies over the Missouri River and upper Mississippi River subbasins; on the lower Ohio River, the month leading up to a flood is characterized by anomalously strong Pacific and Atlantic subtropical highs and positive moisture anomalies over the Ohio River subbasin. Both of these mechanisms result in sustained advection of moisture from the Gulf of Mexico that converges over the continental interior in the weeks preceding a flood. These mechanisms represent the dominant atmospheric patterns associated with large floods (>10-yr recurrence interval) on the lower reaches of the tributaries examined here, but we note the variation among individual events (Figs. S1 and S2 in the online supplemental material) and that other atmospheric patterns can generate large precipitation events in these regions and may be more important for triggering floods on the upper reaches of these tributaries where drainage areas are smaller (Hirschboeck 1988; Smith et al. 2011; Zhang and Villarini 2019). While these large-scale atmospheric patterns trigger floods in the weeks prior to an event, we turn next to major modes of climate variability and their influence on flood occurrence to identify precursors that prime the basin in the months leading up to a flood.

## 5. Ocean–atmosphere forcing of floods

Over interannual time scales, flood occurrence on the lower Missouri and Ohio Rivers is related to the evolution of tropical Pacific Ocean sea surface temperature anomalies—particularly the El Niño–Southern Oscillation (Fig. 5). For lower Missouri River floods, the mean Niño-3.4 index of the 10 largest floods begins to increase 12 months before peak discharge, exceeding the 90% confidence interval beginning four months prior to the event through to the event itself (Fig. 5a). The opposite pattern occurs in the months leading up to lower Ohio River floods, where the mean Niño-3.4 index of the 10 largest floods drops below the 90% confidence interval six months before peak discharge (Fig. 5b). These findings imply that, on aggregate, floods on the lower Missouri River are preceded by an anomalously warm eastern equatorial Pacific, while floods on the lower Ohio River are preceded by an anomalously cold eastern equatorial tropical Pacific in the months before peak flow. We note that the evolution of the Niño-3.4 index differs among the events evaluated here, with the timing and magnitude of warm or cool sea surface temperature anomalies varying among events (Fig. S3 in the online supplemental material), implying that ENSO represents a mechanism that alters the probability of flood occurrence through its influence on antecedent soil moisture (Muñoz and Dee 2017) but is not a deterministic precursor of flooding. For the 10 lower Missouri River floods considered here, 7 (70%) are preceded by El Niño events (defined here as  $\geq 3$  consecutive months with Niño-3.4  $\geq +0.5$ )

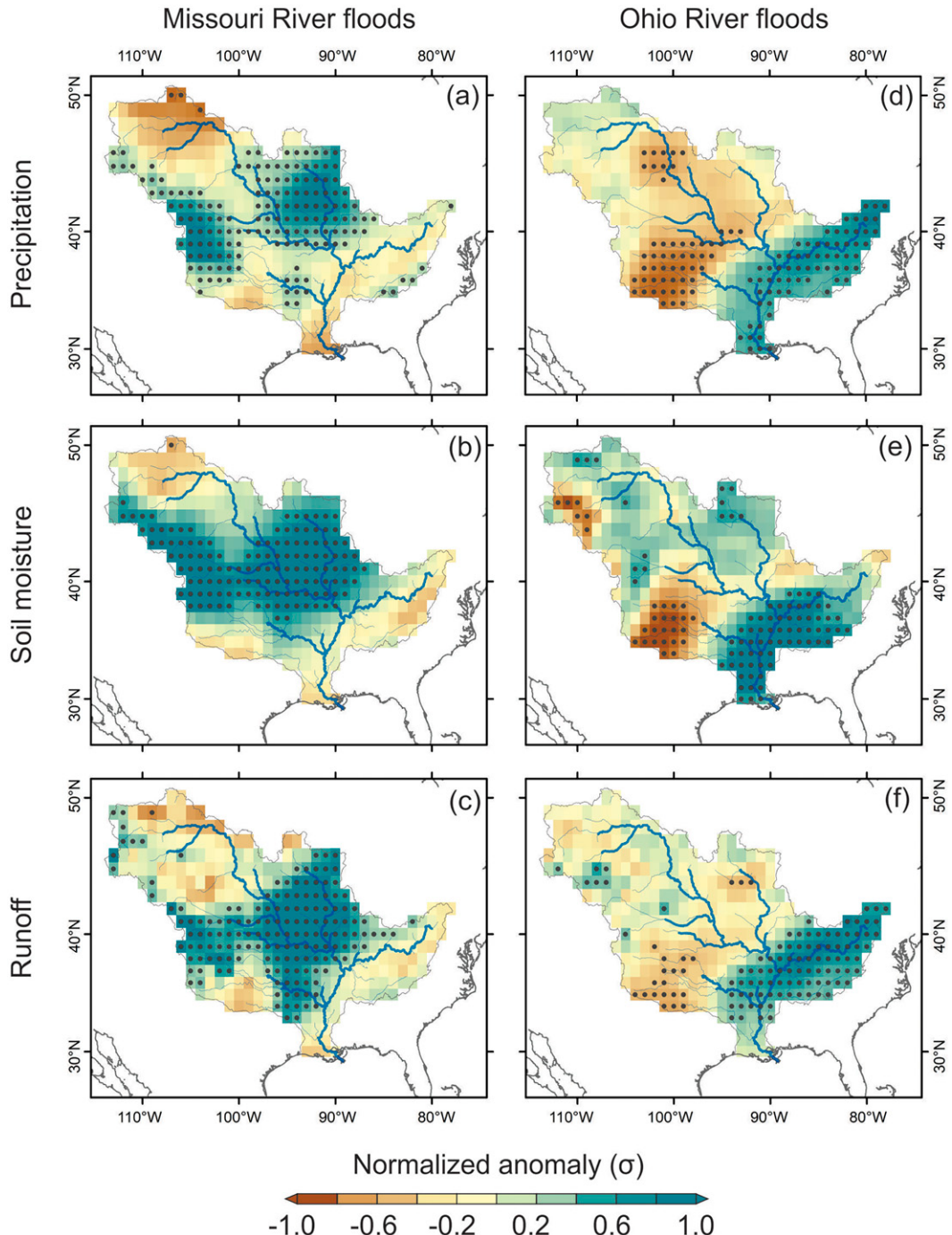


FIG. 4. Hydrologic anomalies in the month prior to peak discharge for the 10 largest floods on (a)–(c) the lower Missouri and (d)–(f) Ohio Rivers, including (top) precipitation, (middle) soil moisture (0–40 cm), and (bottom) runoff. All fields are expressed as standardized anomalies in terms of standard deviations  $\sigma$  from the long-term monthly mean (1981–2010). Stippling denotes composite anomalies that exceed the 90% confidence interval.

in the 18 months before the flood (i.e., floods in 1993, 1903, 1995, 1943, 1986, 2017, and 1973); a lower proportion (50%) of La Niña events (defined here as  $\geq 3$  consecutive months with  $\text{Niño-3.4} \geq -0.5$ ) precede lower Ohio River floods (i.e., floods in 1884, 1964, 1883, 1997, 1907). The evolution of ENSO differs

for individual events, with El Niño/La Niña conditions (i.e., anomalies of  $\pm 0.5^\circ\text{C}$ ) occurring at different times prior to the event. The long residence time of soil water and groundwater means that the influence of ENSO on antecedent moisture persists for months after an El Niño/La Niña event

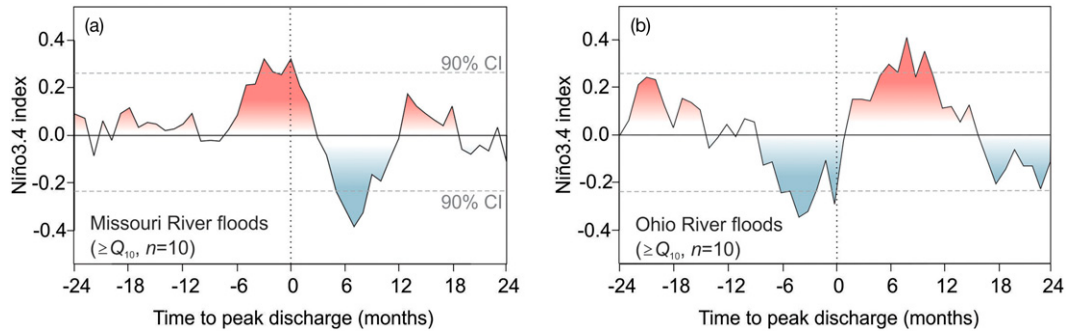


FIG. 5. Evolution of ENSO (Niño3.4 index) in the 24 months before and after peak discharge for the 10 largest floods on the (a) lower Missouri River and (b) lower Ohio River.

occurs (Chen and Kumar 2002; Lo and Famiglietti 2010; Reager et al. 2014). These findings—that El Niño and La Niña events often precede large floods on the lower Missouri and Ohio Rivers, respectively—implicate El Niño–Southern Oscillation in mediating flood occurrence on these rivers over interannual time scales and extend prior work linking the effect of El Niño events on antecedent soil moisture and enhanced flood hazard on the lower Mississippi River (Muñoz and Dee 2017).

Given the geopotential height and wind anomalies associated with these floods identified in section 4, we also examined the evolution of GPLJJ and NAO in the weeks preceding and following the largest floods on the lower Missouri and Ohio Rivers, respectively (Fig. 6). For lower Missouri River floods, the aggregate GPLJJ index consistently exceeds the 90% confidence interval beginning around 20 days prior to peak discharge through to the flood event itself (Fig. 6a). For lower Ohio River floods, the aggregate NAO index of the 10 largest floods exceeds the 90% confidence interval beginning around 25 days prior to peak discharge and drops below this significance threshold 5 days prior to the flood event (Fig. 6b). At an individual event scale, positive GPLJJ index values occur in the weeks prior to all lower Missouri River floods (Fig. S4a in the online supplemental material) and positive NAO values precede all lower Ohio River floods (Fig. S4b). A positive

GPLJJ index, a measure of lower-level (850 hPa) meridional wind anomalies over the southern Great Plains, reflects the strong and directed southerly winds off the Gulf of Mexico observed in the month prior to lower Missouri River floods (Fig. 2). A positive NAO, indicating a strong sea level pressure difference between the North Atlantic subtropical high and Icelandic low (Hurrell et al. 2001), is similar to the atmospheric pattern that triggers lower Ohio River floods (Fig. 3) that features an anomalously strong North Atlantic subtropical high and promotes advection and convergence of moisture from the Gulf of Mexico. As atmospheric modes of variability, the GPLJJ and NAO indices exhibit higher variance than El Niño–Southern Oscillation and thus offer shorter-term predictive value as a flood precursor. Our analyses imply that these atmospheric processes work in concert with oceanic forcing originating in the Pacific to mediate flood occurrence over the major tributaries of the Mississippi River basin.

We propose that floods on the major tributaries of the Mississippi River system are mediated by a two-phase process, where antecedent soil moisture mediated by ENSO in the months preceding an event primes the basin to be vulnerable to flooding, while atmospheric mechanisms (i.e., GPLJJ and NAO indices) provide the “spark”—an influx of precipitation in the weeks leading up to a flood that generates large amounts of runoff and enhances river discharge.

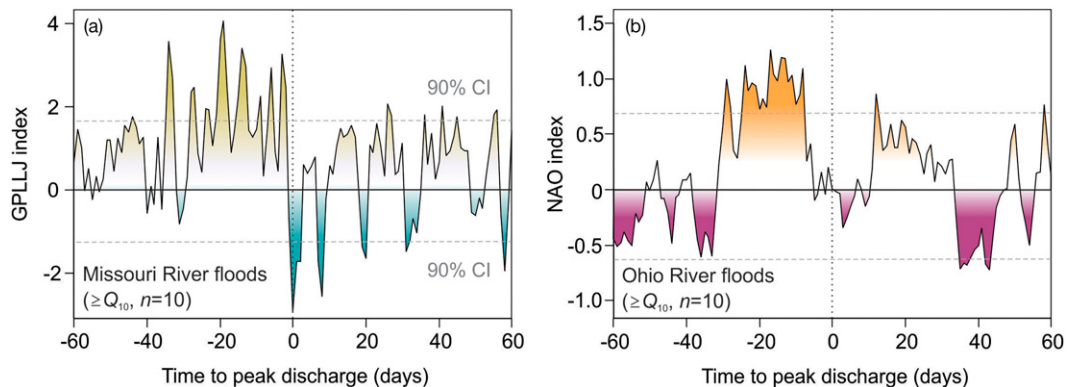


FIG. 6. Evolution of the (a) GPLJJ index and (b) NAO index in the 60 days before and after peak discharge for the 10 largest floods on the lower Missouri River and lower Ohio River.

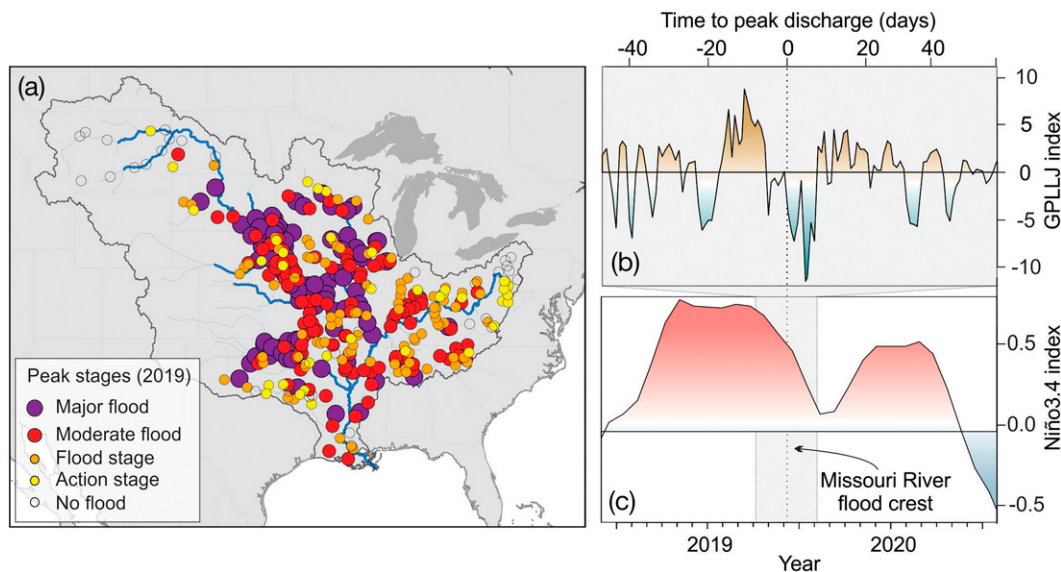


FIG. 7. Hydroclimatic characteristics of the 2019 Missouri–Mississippi River floods: (a) peak stage categories for the 2019 water year for all moderate to large rivers (peak discharge  $> 560 \text{ m}^3 \text{ s}^{-1}$ ); (b) daily GPLJJ index prior to and following flood crest on the lower Missouri River at Hermann on 8 Jun 2019; (c) Niño-3.4 index (June 2018–June 2020).

This same ENSO-priming mechanism has previously been identified on the lower Mississippi River (Muñoz and Dee 2017), and here we propose that it extends to the other major tributaries of the Mississippi River basin. Through its influence on the strength and position of the North Atlantic subtropical high, the NAO regulates precipitation over the eastern and central parts of the Mississippi River basin, explaining why positive departures of the NAO tend to precede major floods on the lower Ohio River. On the lower Missouri River, where floods tend to occur in the spring and summer months, it is a strong Great Plains low-level jet that most often triggers major floods on this tributary. These atmospheric flood triggering mechanisms—namely the strengths of the NAO and GPLJJ—are themselves influenced by modes of ocean–atmosphere variability (Robertson et al. 2000; Walter and Graf 2002; Krishnamurthy et al. 2015). The GPLJJ, in particular, is sensitive to oceanic forcing, with a stronger GPLJJ in boreal spring linked to La Niña while a stronger GPLJJ in boreal summer associated with El Niño (Krishnamurthy et al. 2015), as well as the contrasts in sea surface temperature anomalies between the tropical Pacific and sea surface temperature contrasts and North Atlantic (Malloy and Kirtman 2020).

## 6. 2019 and 2021 floods in hindsight

Major floods occurred within the Mississippi River basin in the water years of 2019 (Fig. 7) and 2021 (Fig. 8) that illustrate the contrasting mechanisms that generate floods across this basin. In the spring and summer of 2019, major flooding occurred primarily along the Missouri and Mississippi Rivers following an El Niño event that began in the autumn of 2018 (Fig. 7). During the 2019 water year, 57% of all gauges

on moderate to large rivers (peak discharge  $> 560 \text{ m}^3 \text{ s}^{-1}$ ;  $n = 419$ ) recorded a moderate or major flood stage, with these floods occurring principally along the Missouri, Arkansas, and Mississippi Rivers and their tributaries. These floods began in the spring of 2019, when a series of heavy precipitation events on saturated and/or frozen soils increased river stages along the lower Missouri and Mississippi Rivers (Pal et al. 2020). Positive GPLJJ index values preceded the flood crest on the lower Missouri River by 3 weeks. Despite flooding over the western and central portions of the Mississippi River basin, flooding along the lower Ohio River was short-lived and moderate. In contrast to the 2019 floods, flooding in the winter and spring of 2020/21 occurred primarily within the Ohio River basin and was preceded by a La Niña event that began in the autumn of 2020 (Fig. 8). During the 2021 floods, 21% of all gauges on moderate to large rivers recorded a moderate or major flood stage, with the majority of these floods occurring within the Ohio, lower Mississippi, and Arkansas subbasins. Positive NAO index values occurred 2 weeks prior to the flood crest on the lower Ohio River.

The pattern of the 2019 and 2021 floods—with major flooding concentrated over the Missouri and upper Mississippi subbasins (2019) and Ohio subbasin (2021)—is consistent with the oceanic and atmospheric mechanisms that we propose regulate flood hazard within the Mississippi River basin. Beginning in the autumn prior to the floods, ENSO generated positive precipitation anomalies that saturated soils and served to prime the western (2019) or eastern (2021) tributary basins to be susceptible to flooding. Then, in the following spring, a series of heavy precipitation events associated with a positive GPLJJ (2019) and NAO (2021) generated large amounts of runoff that contributed to major flooding along

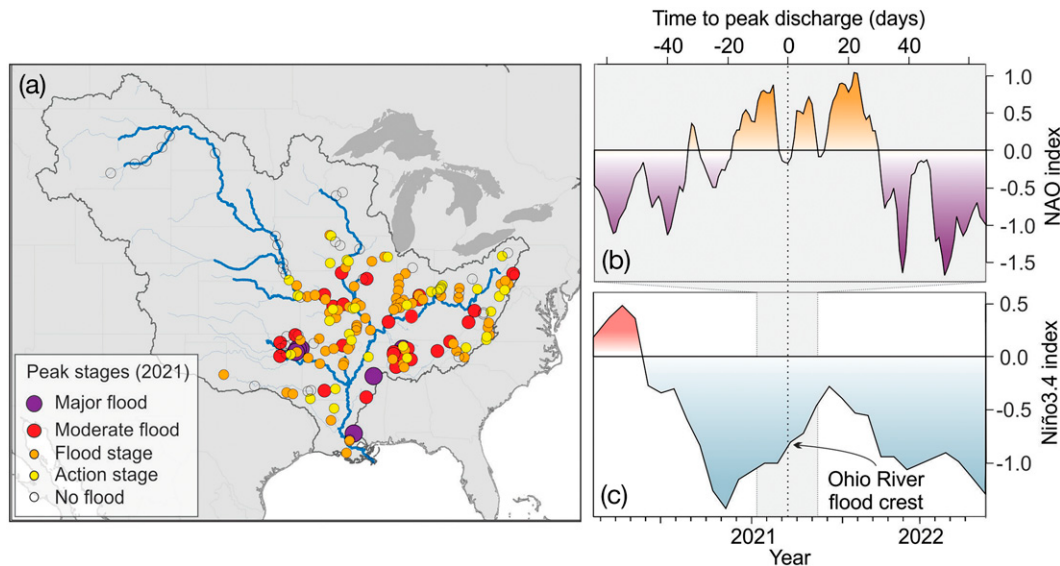


FIG. 8. Hydroclimatic characteristics of the 2021 Ohio River floods: (a) peak stage categories for the 2021 water year for all moderate to large rivers (peak discharge  $> 560 \text{ m}^3 \text{ s}^{-1}$ ); (b) daily NAO index prior to and following flood crest on the lower Ohio River at Louisville on 6 Mar 2021; (c) Niño-3.4 index (March 2020–March 2022).

these tributaries. Spring flood forecasts issued in late March by the National Weather Service in 2019 and 2021 correctly identified observed patterns of flooding (NWS 2019, 2021), providing days to weeks of lead time for the preparation of temporary flood defenses and other mitigation strategies. Our study implies that the formation of El Niño conditions in the autumn of 2018 and La Niña conditions in the autumn of 2020 signaled elevated flood hazard along the lower Missouri River and Ohio Rivers, respectively—a finding that could have added several months of lead time that could be used to regulate reservoir releases, procure and deploy temporary flood mitigation infrastructure, and develop emergency response plans.

## 7. Conclusions

Our results provide a consolidated characterization of the contrasting atmospheric and oceanic mechanisms that generate floods along the principal tributaries of the Mississippi River basin—rivers that form a critical economic corridor for North America. By integrating a climate reanalysis and stream gauge records to examine the hydroclimatology of the largest historical floods on the lower Missouri and Ohio Rivers, we identify the following: 1) the atmospheric mechanisms associated with moisture advection and convergence that trigger high-magnitude floods along these rivers weeks in advance of peak discharge; 2) the role of the El Niño–Southern Oscillation in mediating antecedent moisture across much of the Mississippi River basin in the months prior to peak discharge. Our findings harbor implications for improving long-range probabilistic flood forecasts, and we note the potential for the interaction of ENSO with other modes of climate variability (Meehl and Teng 2007; Zhou et al. 2014) and variability of ENSO itself (Newman et al. 2011;

Luo et al. 2022) to further enhance or suppress flood hazard on these rivers. We also note the potential for land use and river management to exacerbate or ameliorate river stages during a flood independently of climate variability or change (Pinter et al. 2008; Frans et al. 2013). Our work highlights the value of examining commonalities among multiple historical flood events to understand the hydroclimatology of riverine flooding by using publicly available climate reanalysis datasets.

**Acknowledgments.** We thank Sylvia Dee, Trevor Porter, Joeri Reinders, Jessica Tierney, and Charlotte Wiman for discussion and comments on this work. This project was supported by grants from the U.S. National Science Foundation (EAR-1804107 and AGS-2147782).

**Data availability statement.** All data used in this study are publicly available: Twentieth Century Reanalysis, V3 ([https://psl.noaa.gov/data/gridded/data.20thC\\_ReanV3.html](https://psl.noaa.gov/data/gridded/data.20thC_ReanV3.html)); Extended Reconstructed Sea Surface Temperature, ERSST v5 (<https://psl.noaa.gov/data/gridded/data.noaa.ersst.v5.html>); and U.S. Geological Survey (USGS) water data for the nation (<https://waterdata.usgs.gov/nwis>).

## REFERENCES

- Algarra, I., J. Eiras-Barca, G. Miguez-Macho, R. Nieto, and L. Gimeno, 2019: On the assessment of the moisture transport by the Great Plains low-level jet. *Earth Syst. Dyn.*, **10**, 107–119, <https://doi.org/10.5194/esd-10-107-2019>.
- Arritt, R. W., T. D. Rink, M. Segal, D. P. Todey, C. A. Clark, M. J. Mitchell, and K. M. Labas, 1997: The Great Plains low-level jet during the warm season of 1993. *Mon. Wea. Rev.*, **125**,

- 2176–2192, [https://doi.org/10.1175/1520-0493\(1997\)125<2176:TGPLLJ>2.0.CO;2](https://doi.org/10.1175/1520-0493(1997)125<2176:TGPLLJ>2.0.CO;2).
- Camillo, C. A., 2012: *Divine Providence: The 2011 Flood in the Mississippi River and Tributaries Project*. Mississippi River Commission, 312 pp.
- Chen, J., and P. Kumar, 2002: Role of terrestrial hydrologic memory in modulating ENSO impacts in North America. *J. Climate*, **15**, 3569–3585, [https://doi.org/10.1175/1520-0442\(2003\)015<3569:ROTHMI>2.0.CO;2](https://doi.org/10.1175/1520-0442(2003)015<3569:ROTHMI>2.0.CO;2).
- Coats, S., J. E. Smerdon, B. I. Cook, R. Seager, E. R. Cook, and K. J. Anchukaitis, 2016: Internal ocean-atmosphere variability drives megadroughts in western North America. *Geophys. Res. Lett.*, **43**, 9886–9894, <https://doi.org/10.1002/2016GL070105>.
- Cook, B. I., R. Seager, and R. L. Miller, 2011: On the causes and dynamics of the early twentieth-century North American pluvial. *J. Climate*, **24**, 5043–5060, <https://doi.org/10.1175/2011JCLI4201.1>.
- , J. E. Smerdon, R. Seager, and E. R. Cook, 2014: Pancontinental droughts in North America over the last millennium. *J. Climate*, **27**, 383–397, <https://doi.org/10.1175/JCLI-D-13-00100.1>.
- Cook, E. R., R. Seager, M. A. Cane, and D. W. Stahle, 2007: North American drought: Reconstructions, causes, and consequences. *Earth-Sci. Rev.*, **81**, 93–134, <https://doi.org/10.1016/j.earscirev.2006.12.002>.
- Cropper, T., E. Hanna, M. A. Valente, and T. Jónsson, 2015: A daily Azores–Iceland North Atlantic oscillation index back to 1850. *Geosci. Data J.*, **2**, 12–24, <https://doi.org/10.1002/gdj3.23>.
- Dirmeyer, P. A., and J. L. Kinter III, 2009: The “Maya Express”: Floods in the U.S. Midwest. *Eos, Trans. Amer. Geophys. Union*, **90**, 101–102, <https://doi.org/10.1029/2009EO120001>.
- , and —, 2010: Floods over the U.S. Midwest: A regional water cycle perspective. *J. Hydrometeor.*, **11**, 1172–1181, <https://doi.org/10.1175/2010JHM1196.1>.
- Enfield, D. B., A. M. Mestas-Nuñez, and P. J. Trimble, 2001: The Atlantic multidecadal oscillation and its relation to rainfall and river flows in the continental U.S. *Geophys. Res. Lett.*, **28**, 2077–2080, <https://doi.org/10.1029/2000GL012745>.
- Feng, S., Q. Hu, and R. J. Oglesby, 2011: Influence of Atlantic sea surface temperatures on persistent drought in North America. *Climate Dyn.*, **37**, 569–586, <https://doi.org/10.1007/s00382-010-0835-x>.
- Frans, C., E. Istanbulluoglu, V. Mishra, F. Munoz-Arriola, and D. P. Lettenmaier, 2013: Are climatic or land cover changes the dominant cause of runoff trends in the Upper Mississippi River Basin? *Geophys. Res. Lett.*, **40**, 1104–1110, <https://doi.org/10.1002/grl.50262>.
- Hamlet, A. F., and D. P. Lettenmaier, 1999: Columbia River streamflow forecasting based on ENSO and PDO climate signals. *J. Water Resour. Plann. Manage.*, **125**, 333–341, [https://doi.org/10.1061/\(ASCE\)0733-9496\(1999\)125:6\(333\)](https://doi.org/10.1061/(ASCE)0733-9496(1999)125:6(333)).
- Harding, K. J., and P. K. Snyder, 2015: The relationship between the Pacific–North American teleconnection pattern, the Great Plains low-level jet, and north central U.S. heavy rainfall events. *J. Climate*, **28**, 6729–6742, <https://doi.org/10.1175/JCLI-D-14-00657.1>.
- Helfand, H. M., and S. D. Schubert, 1995: Climatology of the simulated Great Plains low-level jet and its contribution to the continental moisture budget of the United States. *J. Climate*, **8**, 784–806, [https://doi.org/10.1175/1520-0442\(1995\)008<0784:COTSGP>2.0.CO;2](https://doi.org/10.1175/1520-0442(1995)008<0784:COTSGP>2.0.CO;2).
- Higgins, R. W., Y. Yao, E. S. Yarosh, J. E. Janowiak, and K. C. Mo, 1997: Influence of the Great Plains low-level jet on summertime precipitation and moisture transport over the central United States. *J. Climate*, **10**, 481–507, [https://doi.org/10.1175/1520-0442\(1997\)010<0481:IOTGPL>2.0.CO;2](https://doi.org/10.1175/1520-0442(1997)010<0481:IOTGPL>2.0.CO;2).
- Hirschboeck, K. K., 1988: Flood hydroclimatology. *Flood Geomorphology*, V. R. Baker, R. C. Kochel, and P. C. Palton, Eds., John Wiley and Sons, 27–49.
- Hoerling, M., J. Eischeid, and R. Webb, 2013: Understanding and explaining climate extremes in the Missouri River basin associated with the 2011 flooding. NOAA Climate Assessment Rep., 34 pp., <https://www.esrl.noaa.gov/psd/csi/factsheets/pdf/noaa-mrb-climate-assessment-report.pdf>.
- Huang, B., and Coauthors, 2017: Extended Reconstructed Sea Surface Temperature, version 5 (ERSSTv5): Upgrades, validations, and intercomparisons. *J. Climate*, **30**, 8179–8205, <https://doi.org/10.1175/JCLI-D-16-0836.1>.
- Hurrell, J. W., Y. Kushnir, and M. Visbeck, 2001: The North Atlantic oscillation. *Science*, **291**, 603–605, <https://doi.org/10.1126/science.1058761>.
- , —, G. Ottersen, and M. Visbeck, 2003: An overview of the North Atlantic Oscillation. *The North Atlantic Oscillation: Climatic Significance and Environmental Impact*, *Geophys. Monogr.*, Vol. 134, Amer. Geophys. Union, 1–35, <https://doi.org/10.1029/134GM01>.
- Keown, M. P., E. A. Dardeau Jr., and E. M. Causey, 1986: Historic trends in the sediment flow regime of the Mississippi River. *Water Resour. Res.*, **22**, 1555–1564, <https://doi.org/10.1029/WR022i011p01555>.
- Knox, J. C., 2007: The Mississippi River system. *Large Rivers: Geomorphology and Management*, A. Gupta, Ed., John Wiley and Sons, 145–182, <https://doi.org/10.1002/9780470723722.ch9>.
- Krishnamurthy, L., G. A. Vecchi, R. Msadek, A. Wittenberg, T. L. Delworth, and F. Zeng, 2015: The seasonality of the Great Plains low-level jet and ENSO relationship. *J. Climate*, **28**, 4525–4544, <https://doi.org/10.1175/JCLI-D-14-00590.1>.
- Kunkel, K. E., S. A. Changnon, and J. R. Angel, 1994: Climatic aspects of the 1993 upper Mississippi River basin flood. *Bull. Amer. Meteor. Soc.*, **75**, 811–822, [https://doi.org/10.1175/1520-0477\(1994\)075<0811:CAOTUM>2.0.CO;2](https://doi.org/10.1175/1520-0477(1994)075<0811:CAOTUM>2.0.CO;2).
- Li, W., L. Li, R. Fu, Y. Deng, and H. Wang, 2011: Changes to the North Atlantic subtropical high and its role in the intensification of summer rainfall variability in the southeastern United States. *J. Climate*, **24**, 1499–1506, <https://doi.org/10.1175/2010JCLI3829.1>.
- Lincoln, W. S., and D. Graschel, 2016: 2016 forecast verifications at the Lower Mississippi River Forecast Center using varying QPF. LMRFC Tech. Rep., 25 pp., [http://www.weather.gov/media/lmrfc/tech/2016\\_07\\_QPF\\_forecast\\_verifications.pdf](http://www.weather.gov/media/lmrfc/tech/2016_07_QPF_forecast_verifications.pdf).
- , and —, 2018: 2018 Analysis of gridded precipitation estimation techniques at the Lower Mississippi River Forecast Center. LMRFC Tech. Rep., 10 pp., [http://www.weather.gov/media/lmrfc/tech/2018\\_Analysis\\_QPE\\_Techniques.pdf](http://www.weather.gov/media/lmrfc/tech/2018_Analysis_QPE_Techniques.pdf).
- Lo, M.-H., and J. S. Famiglietti, 2010: Effect of water table dynamics on land surface hydrologic memory. *J. Geophys. Res.*, **115**, D22118, <https://doi.org/10.1029/2010JD014191>.
- Lott, G. A., and V. A. Myers, 1956: Meteorology of flood-producing storms in the Mississippi River basin. U.S. Government Printing Office Hydrometeorological Rep. 34, 226 pp.
- Luo, X., S. Dee, S. Stevenson, Y. Okumura, N. Steiger, and L. Parsons, 2022: Last millennium ENSO diversity and North American teleconnections: New insights from paleoclimate data

- assimilation. *Paleoceanogr. Paleoclimatol.*, **37**, e2021PA004283, <https://doi.org/10.1029/2021PA004283>.
- Mallakpour, I., and G. Villarini, 2016: Investigating the relationship between the frequency of flooding over the central United States and large-scale climate. *Adv. Water Resour.*, **92**, 159–171, <https://doi.org/10.1016/j.advwatres.2016.04.008>.
- Malloy, K. M., and B. P. Kirtman, 2020: Predictability of midsummer Great Plains low-level jet and associated precipitation. *Wea. Forecasting*, **35**, 215–235, <https://doi.org/10.1175/WAF-D-19-0103.1>.
- Meehl, G. A., and H. Teng, 2007: Multi-model changes in El Niño teleconnections over North America in a future warmer climate. *Climate Dyn.*, **29**, 779–790, <https://doi.org/10.1007/s00382-007-0268-3>.
- Mo, K. C., J. N. Paegle, and R. W. Higgins, 1997: Atmospheric processes associated with summer floods and droughts in the central United States. *J. Climate*, **10**, 3028–3046, [https://doi.org/10.1175/1520-0442\(1997\)010<3028:APAWSF>2.0.CO;2](https://doi.org/10.1175/1520-0442(1997)010<3028:APAWSF>2.0.CO;2).
- Muñoz, S. E., and S. G. Dee, 2017: El Niño increases the risk of lower Mississippi River flooding. *Sci. Rep.*, **7**, 1772, <https://doi.org/10.1038/s41598-017-01919-6>.
- , and Coauthors, 2018: Climatic control of Mississippi River flood hazard amplified by river engineering. *Nature*, **556**, 95–98, <https://doi.org/10.1038/nature26145>.
- , T. J. Porter, A. Bakkelund, J. Nusbaumer, S. G. Dee, B. Hamilton, L. Giosan, and J. E. Tierney, 2020: Lipid biomarker record documents hydroclimatic variability of the Mississippi River basin during the Common Era. *Geophys. Res. Lett.*, **47**, e2020GL087237, <https://doi.org/10.1029/2020GL087237>.
- Nakamura, J., U. Lall, Y. Kushnir, A. W. Robertson, and R. Seager, 2013: Dynamical structure of extreme floods in the U.S. Midwest and the United Kingdom. *J. Hydrometeor.*, **14**, 485–504, <https://doi.org/10.1175/JHM-D-12-059.1>.
- Newman, M., S.-I. Shin, and M. A. Alexander, 2011: Natural variation in ENSO flavors. *Geophys. Res. Lett.*, **38**, L14705, <https://doi.org/10.1029/2011GL047658>.
- NCEI, 2021: U.S. billion-dollar weather and climate disasters. NOAA, accessed 5 May 2021, <https://doi.org/10.25921/stkw-7w73>.
- NOAA, 2016: The national water model: Improving NOAA's water prediction service. NOAA, 2 pp., <https://water.noaa.gov/documents/wrn-national-water-model.pdf>.
- NWS, 2019: 2019 spring flood and water resource outlook. NOAA, accessed 5 May 2021, [https://www.weather.gov/dvn/2019\\_springfloodoutlook](https://www.weather.gov/dvn/2019_springfloodoutlook).
- , 2021: 2021 spring flood and water resource outlook. NOAA, accessed 5 May 2021, [https://www.weather.gov/dvn/2021\\_springfloodoutlook](https://www.weather.gov/dvn/2021_springfloodoutlook).
- Pal, S., T. R. Lee, and N. E. Clark, 2020: The 2019 Mississippi and Missouri river flooding and its impact on atmospheric boundary layer dynamics. *Geophys. Res. Lett.*, **47**, e2019GL086933, <https://doi.org/10.1029/2019GL086933>.
- Parrett, C., N. B. Melcher, and R. W. James Jr., 1993: Flood discharges in the upper Mississippi River basin, 1993. USGS Rep. 1120, 14 pp., <https://doi.org/10.3133/cir1120A>.
- Pinter, N., A. A. Jemberie, J. W. F. Remo, R. A. Heine, and B. S. Ickes, 2008: Flood trends and river engineering on the Mississippi River system. *Geophys. Res. Lett.*, **35**, L23404, <https://doi.org/10.1029/2008GL035987>.
- Reager, J. T., B. F. Thomas, and J. S. Famiglietti, 2014: River basin flood potential inferred using GRACE gravity observations at several months lead time. *Nat. Geosci.*, **7**, 588–592, <https://doi.org/10.1038/ngeo2203>.
- Robertson, A. W., C. R. Mechoso, and Y.-J. Kim, 2000: The influence of Atlantic sea surface temperature anomalies on the North Atlantic oscillation. *J. Climate*, **13**, 122–138, [https://doi.org/10.1175/1520-0442\(2000\)013<0122:TIOASS>2.0.CO;2](https://doi.org/10.1175/1520-0442(2000)013<0122:TIOASS>2.0.CO;2).
- Ropelewski, C. F., and M. S. Halpert, 1986: North American precipitation and temperature patterns associated with the El Niño/Southern Oscillation (ENSO). *Mon. Wea. Rev.*, **114**, 2352–2362, [https://doi.org/10.1175/1520-0493\(1986\)114<2352:NAPATP>2.0.CO;2](https://doi.org/10.1175/1520-0493(1986)114<2352:NAPATP>2.0.CO;2).
- Schöngart, J., and W. J. Junk, 2007: Forecasting the flood-pulse in central Amazonia by ENSO-indices. *J. Hydrol.*, **335**, 124–132, <https://doi.org/10.1016/j.jhydrol.2006.11.005>.
- Seager, R., Y. Kushnir, C. Herweijer, N. Naik, and J. Velez, 2005: Modeling of tropical forcing of persistent droughts and pluvials over western North America: 1856–2000. *J. Climate*, **18**, 4065–4088, <https://doi.org/10.1175/JCLI3522.1>.
- Slivinski, L. C., and Coauthors, 2019: Towards a more reliable historical reanalysis: Improvements for version 3 of the Twentieth Century Reanalysis system. *Quart. J. Roy. Meteor. Soc.*, **145**, 2876–2908, <https://doi.org/10.1002/qj.3598>.
- Smith, J. A., and M. L. Baeck, 2015: “Prophetic vision, vivid imagination”: The 1927 Mississippi River flood. *Water Resour. Res.*, **51**, 9964–9994, <https://doi.org/10.1002/2015WR017927>.
- , —, A. A. Ntelekos, G. Villarini, and M. Steiner, 2011: Extreme rainfall and flooding from orographic thunderstorms in the central Appalachians. *Water Resour. Res.*, **47**, W04514, <https://doi.org/10.1029/2010WR010190>.
- Smith, L. M., and B. R. Winkley, 1996: The response of the lower Mississippi River to river engineering. *Eng. Geol.*, **45**, 433–455, [https://doi.org/10.1016/S0013-7952\(96\)00025-7](https://doi.org/10.1016/S0013-7952(96)00025-7).
- Therrell, M. D., and M. B. Bialecki, 2015: A multi-century tree-ring record of spring flooding on the Mississippi River. *J. Hydrol.*, **529**, 490–498, <https://doi.org/10.1016/j.jhydrol.2014.11.005>.
- Thomson, A. M., R. A. Brown, N. J. Rosenberg, R. C. Izaurralde, D. M. Legler, and R. Srinivasan, 2003: Simulated impacts of El Niño/southern oscillation on United States water resources. *J. Amer. Water Resour. Assoc.*, **39**, 137–148, <https://doi.org/10.1111/j.1752-1688.2003.tb01567.x>.
- Trenberth, K. E., 1997: The definition of El Niño. *Bull. Amer. Meteor. Soc.*, **78**, 2771–2778, [https://doi.org/10.1175/1520-0477\(1997\)078<2771:TDOENO>2.0.CO;2](https://doi.org/10.1175/1520-0477(1997)078<2771:TDOENO>2.0.CO;2).
- USGS, 2021: USGS water data for the nation. USGS, accessed 15 March 2021, <https://waterdata.usgs.gov/nwis>.
- Walter, K., and H.-F. Graf, 2002: On the changing nature of the regional connection between the North Atlantic oscillation and sea surface temperature. *J. Geophys. Res.*, **107**, 4338, <https://doi.org/10.1029/2001JD000850>.
- Wang, G., and E. A. Eltahir, 1999: Use of ENSO information in medium- and long-range forecasting of the Nile floods. *J. Climate*, **12**, 1726–1737, [https://doi.org/10.1175/1520-0442\(1999\)012<1726:UEOIIM>2.0.CO;2](https://doi.org/10.1175/1520-0442(1999)012<1726:UEOIIM>2.0.CO;2).
- Wang, S.-Y., and T.-C. Chen, 2009: The late-spring maximum of rainfall over the U.S. central plains and the role of the low-level jet. *J. Climate*, **22**, 4696–4709, <https://doi.org/10.1175/2009JCLI2719.1>.
- Weaver, S. J., and S. Nigam, 2008: Variability of the Great Plains low-level jet: Large-scale circulation context and hydroclimate impacts. *J. Climate*, **21**, 1532–1551, <https://doi.org/10.1175/2007JCLI1586.1>.

- Wise, E. K., C. A. Woodhouse, G. J. McCabe, G. T. Pederson, and J.-M. St-Jacques, 2018: Hydroclimatology of the Missouri River basin. *J. Hydrometeor.*, **19**, 161–182, <https://doi.org/10.1175/JHM-D-17-0155.1>.
- Zhang, W., and G. Villarini, 2019: On the weather types that shape the precipitation patterns across the U.S. Midwest. *Climate Dyn.*, **53**, 4217–4232, <https://doi.org/10.1007/s00382-019-04783-4>.
- Zhou, Z.-Q., S.-P. Xie, X.-T. Zheng, Q. Liu, and H. Wang, 2014: Global warming-induced changes in El Niño teleconnections over the North Pacific and North America. *J. Climate*, **27**, 9050–9064, <https://doi.org/10.1175/JCLI-D-14-00254.1>.